

# Comparative Evaluation for Torque Control Strategies of Interior Permanent Magnet Synchronous Motor for Electric Vehicles

Hanaa Elsherbiny<sup>1\*</sup>, Mohamed Kamal Ahmed<sup>1</sup>, Mahmoud A. Elwany<sup>1</sup>

<sup>1</sup> Department of Electrical Engineering, Faculty of Engineering, El-Azhar University, Nasr City, 11751 Cairo, P.O.B. 11751, Egypt

\* Corresponding author, e-mail: [Hanaaelsherbiny.60@azhar.edu.eg](mailto:Hanaaelsherbiny.60@azhar.edu.eg)

Received: 15 June 2020, Accepted: 07 September 2020, Published online: 06 July 2021

## Abstract

This paper presents a detailed analysis and comparative investigation for the torque control techniques of interior permanent magnet synchronous motor (IPMSM) for electric vehicles (EVs). The study involves the field-oriented control (FOC), direct torque control (DTC), and model predictive direct torque control (MPDTC) techniques. The control aims to achieve vehicle requirements that involve maximum torque per ampere (MTPA), minimum torque ripples, maximum efficiency, fast dynamics, and wide speed range. The MTPA is achieved by the direct calculation of reference flux-linkage as a function of commanded torque. The calculation of reference flux-linkage is done online by the solution of a quartic equation. Therefore, it is a more practical solution compared to look-up table methods that depend on machine parameters and require extensive offline calculations in advance. For realistic results, the IPMSM model is built considering iron losses. Besides, the IGBTs and diodes losses (conduction and switching losses) in power inverter are modeled and calculated to estimate properly total system efficiency. In addition, a bidirectional dc-dc boost converter is connected to the battery to improve the overall drive performance and achieve higher efficiency values. Also, instead of the conventional PI controller which suffers from parameter variation, the control scheme includes an adaptive fuzzy logic controller (FLC) to provide better speed tracking performance. It also provides a better robustness against disturbance and uncertainties. Finally, a series of simulation results with detailed analysis are executed for a 60 kW IPMSM. The electric vehicle (EV) parameters are equivalent to Nissan Leaf 2018 electric car.

## Keywords

IPMSM, FOC, DTC, MPDTC, MTPA, iron losses, inverter losses

This article was originally published with an error. This version has been corrected/amended in the Corrigendum. Please see the Corrigendum (<https://doi.org/10.3311/PPee.18968>)!

## 1 Introduction

Nowadays, Electric vehicles are gaining an increasing interest. They are the future for green transportation and for establishment of a low-carbon economy [1, 2]. EVs offer many advantages of no emissions, low maintenance, cost-effective, safety drive, popularity, and reduced noise pollution. Besides, they hold a significant potential for improving the local air quality [2–4].

The propulsion system of the EV is comprised of a motor, power converter, and controller. For different types of new energy vehicles, the motor drive system is the core and common technology [2]. For the electric motor of an EV, the most important characteristics are to provide flexible drive control, high efficiency, high reliability, and low acoustic noise. Besides, the fast and robust torque response is essential to meet the commanded instantaneous torque by the driver [4–7].

The permanent magnet synchronous motors (PMSMs) have the best overall performance as the main drive system in EVs [2]. This is mainly due to their superiorities such as small size and weight, wide speed range, low noise, high power density, and high efficiency. They can easily fulfill all the vehicle requirements with a proper torque control [8, 9].

Lately, different torque control techniques named field oriented control (FOC), direct torque control (DTC), and model predictive direct torque control (MPDTC) have been introduced [9–11]. The variety of control techniques helped to introduce a huge number of possibilities for the optimal control of electric machines. However, which technique can provide the best results still an open question, mainly, because the introduced control techniques are performed on different electric machines with

different parameters. The majority of published papers have been immersed to compare the basic DTC with one modified DTC, or to compare the same type of modified DTC schemes [12, 13]. Nonetheless very few have conducted comparison between different types of improved DTC techniques [13–16]. But, the study excluded MPDTC as it is a relatively new method.

The DTC features fast dynamics but has a considerable torque ripple. The ripple can be compensated by certain methods. Increasing the number of voltage vectors is an effective solution that led to the use of multilevel inverters [17]. In [14, 18] a constant switching frequency based DTC scheme is introduced. It obtains the desired torque and flux in one control period using space vector modulator (SVM) to synthesize the suitable voltage vector. On one side, the FOC doesn't have fast dynamics as DTC because it employs a SVM based on PI/PID as current controllers [19]. But, it has a smooth torque-wise. The dynamics of FOC depends on the gains of PI/PID current controllers. Fast dynamics can be achieved but it may lead to undesired overshoot. On the other side, the MPC offers more flexibility and intuition as it uses a mathematical cost-function to attain the control objectives [20–22]. Different system constrains and performance optimization can be achieved easily with the application of the cost-function. Therefore, the control of torque, flux, switching frequency, and the limitation of currents magnitude can be taken into account by the utilization of cost function [23]. Lately, MPC has attracted the research attention because of its high performance as integrated with DTC [20, 24]. In [13, 25], a duty ratio modulation (DRM) method is optimized for further reduction of torque and flux ripples. A fraction of one control period is set for the nonzero voltage vector and the rest of time for the zero-voltage vector. In [26], a hybrid direct torque control based a predictive control is presented for the minimum torque and flux ripples. Recently, in [27, 28], a novel MPTC scheme is proposed using PWM as a powerful alternative compared to the traditional FOC.

High efficiency is basic for EVs to extend driving mileage per charge. It can be achieved with loss minimization that is the core idea of maximum torque per ampere (MTPA) strategies [1, 11]. For PMSM drives, there are several MTPA based torque control strategies. First, a look-up table method is used to generate a relationship between the torque, flux-linkage, and d, q-axes currents. Both the magnet flux-linkage and the d, q-axes inducances affect this relationship [11]. However, the variation of machine parameters due to the magnetic saturation and

temperature effects cannot be included using lookup tables (LUTs). Therefore, as the parameters vary, the LUT solution does not always obtain the MTPA conditions. Another solution is to detect the optimal reference flux successively [29, 30]. This method employs mathematical formulation to estimate the reference stator flux directly from the reference commanded torque using motor model based MTPA conditions. It offers a simple solution that can be easily implemented. Besides, it is a parameter insensitive solution as the variation of motor parameters can be easily included with in the formulations. Hence, it is adopted in this research.

The high-performance drive should always track the desired reference speed even with load impacts, saturation, and parameter variations. The conventional controllers (P, PI and PID) require an accurate model of the control system that gives a full description of system dynamics. Besides, it is a very exhausting task to design such controllers without an accurate system model. Moreover, they require meticulous fine-tuning and cannot cope with the variation of system parameters. Furthermore, the noise, temperature, saturation, and unknown load dynamics affect their performance [31, 32].

In this paper, a detailed analysis and comparative simulation investigation between the FOC, DTC, and MPDTC is achieved. The study is done basically for EV applications. The MTPA, the field weakling, the iron losses, and the inverter losses are considered during the investigation. The results represent an instructive guidance in order to determine the best control scheme that can achieve the desired control objectives.

The rest of this paper is organized as follows: Section II gives the mathematical model for the PMSM model, the voltage source inverter, the EV, the inverter losses, and the performance indices. The reference flux calculation for MTPA is obtained in Section 3. Section 4 shows the basic traction drive topologies for EVs. The speed control based fuzzy logic control (FLC) is contained in Section 5. The FOC, DTC, and MPDTC techniques are explained in Sections 6, 7, and 8, respectively. The simulation results and their discussions are given in Section 9. The conclusion is obtained in Section 10.

## 2 System modeling

### 2.1 PMSM model including iron losses

Fig. 1 shows the d and q-axes equivalent circuits of an IPMSM. The effect of iron and copper losses are represented by the resistances  $R_c$  and  $R_s$ , respectively.

From Fig. 1, the dynamic model of IPMSM in the synchronous rotating dq reference frame can be derived as follows in Eqs. (1) and (2) [33–35]:

$$\frac{di_{md}}{dt} = \frac{1}{L_d} (v_d - R_s i_d + \omega L_q i_{mq}), \quad (1)$$

$$\frac{di_{mq}}{dt} = \frac{1}{L_q} (v_q - R_s i_q - \omega L_d i_{md} - \omega \lambda_{pm}), \quad (2)$$

where  $i_{md}$  and  $i_{mq}$  are  $d$  and  $q$ -axis components of magnetizing currents,  $i_d$  and  $i_q$  are  $d$  and  $q$ -axis components of armature current,  $v_d$  and  $v_q$  are  $d$  and  $q$ -axis components of the terminal voltage,  $L_d$  and  $L_q$  are  $d$  and  $q$ -axis inductances,  $\omega$  is the angular velocity, and  $\lambda_{pm}$  depicts the flux-linkage of permanent magnets.

$$i_d = \frac{1}{R_c} \left( L_d \frac{di_{md}}{dt} - \omega L_q i_{mq} + R_c i_{md} \right), \quad (3)$$

$$i_q = \frac{1}{R_c} \left( L_q \frac{di_{mq}}{dt} + \omega L_d i_{md} + R_c i_{mq} + \omega \lambda_{pm} \right), \quad (4)$$

$$i_{cd} = i_d - i_{md}, \quad i_{cq} = i_q - i_{mq}, \quad (5)$$

$$T_e = \frac{3}{2} p i_{mq} (\lambda_{pm} + (L_d - L_q) i_{md}), \quad (6)$$

where  $i_{cd}$  and  $i_{cq}$  are  $d$  and  $q$ -axis components of iron loss current,  $T_e$  represents the motor torque, and  $p$  is the number of pole pairs.

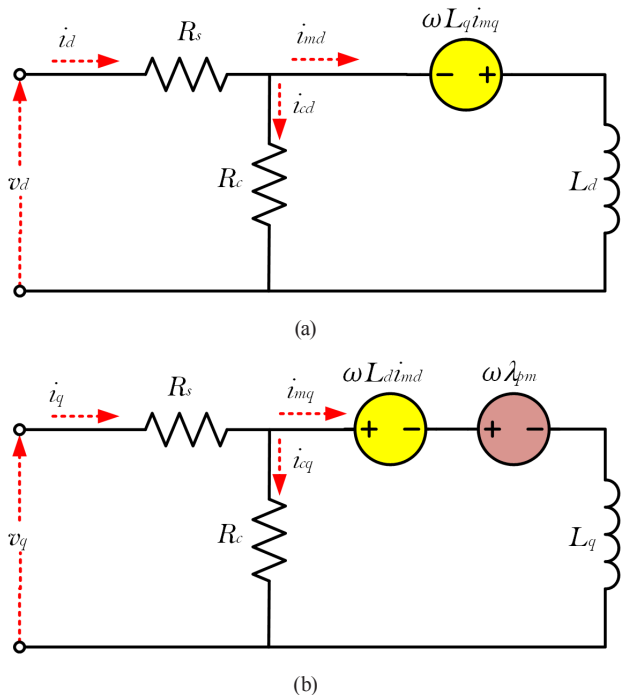


Fig. 1 The  $d$  and  $q$ -axis equivalent circuits of an IPMSM considering iron losses; (a)  $d$ -axis, (b)  $q$ -axis

The mechanical equation (Eq. 7) of the machine is:

$$J \frac{d\omega}{dt} = T_e - T_L - B\omega, \quad (7)$$

where  $J$  is the inertia,  $B$  is the frictional coefficient, and  $T_L$  is the load torque.

The motor copper losses ( $P_{cu}$ ), and the iron loss ( $P_{iron}$ ) can be calculated as follows in Eqs. (8) and (9):

$$P_{cu} = \frac{3}{2} R_s (i_d^2 + i_q^2), \quad (8)$$

$$P_{iron} = \frac{3}{2} R_c (i_{cd}^2 + i_{cq}^2). \quad (9)$$

## 2.2 Modeling of power converter

The commonly used 2-level voltage source inverter (VSI) involves 6 IGBTs and 6 free-wheeling diodes. The IGBTs and diodes are arranged in the form of three half-bridges. The switching state can be defined by the control signals  $S_a$ ,  $S_b$  and  $S_c$  as follows in Eqs. (10) and (11) [19]:

$$S = \frac{3}{2} \left( S_a + S_b e^{\frac{j2\pi}{3}} + S_c e^{\frac{j4\pi}{3}} \right), \quad (10)$$

$$V = S V_{DC}, \quad (11)$$

where  $V_{DC}$  is the DC voltage, and  $V$  is the output voltage vector.

## 2.3 Model of the electric vehicle

The commanded torque of an EV can be calculated based on vehicle dynamics. The forces acting on the vehicle body involve the traction force ( $F_t$ ), rolling resistance from the road surface ( $F_r$ ), aerodynamic resistance ( $F_{aero}$ ), hill climbing resistance ( $F_g$ ), and accelerating resistance ( $F_a$ ) as shown in Fig. 2 and Eq. (12) [2].

$$F_t = \eta_t i_o \frac{T_e}{R_w}, \quad (12)$$

where  $\eta_t$  is the transmission efficiency,  $i_o$  is reduction gear ratio, and  $R_w$  is the wheel radius.

$$F_r = M g f_r, \quad (13)$$

$$F_g = M g \sin \beta, \quad (14)$$

where  $M$  is the vehicle mass,  $g$  is the gravity acceleration,  $f_r$  is the friction rolling coefficient, and  $\beta$  is the slope angle.

$$F_{aero} = \frac{1}{2} \rho A_f C_d V_x^2, \quad (15)$$

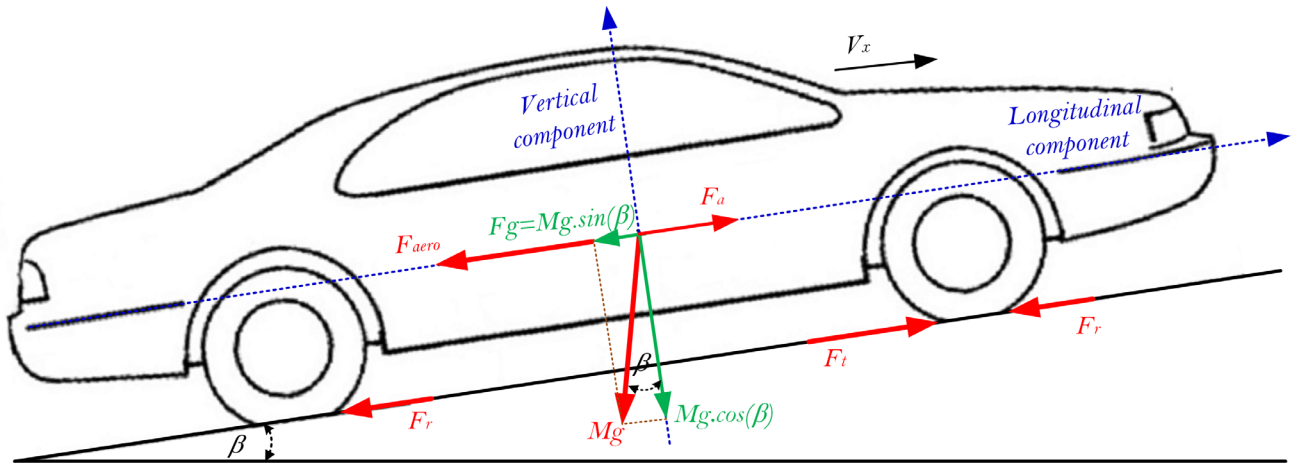


Fig. 2 Forces acting on a vehicle moving uphill

where  $\rho$  represent the air density,  $C_d$  stands for the drag coefficient,  $A_f$  depicts the vehicle frontal area, and  $V_x$  is the vehicle speed.

$$F_a = M \frac{dV_x}{dt}, \quad (16)$$

According to Newton's second law:

$$F_t = F_r + F_{aero} + F_g + F_a. \quad (17)$$

The force balancing equation for a pure EV can be summarized as in Eq. (18).

$$\eta_t i_o \frac{T_e}{R_w} = Mgf_r + \frac{1}{2} \rho A_f C_d V_x^2 + Mg \sin \beta + M \frac{dV_x}{dt}. \quad (18)$$

The motor torque ( $T_e$ ) is inputted to Eq. (18) to output vehicle speed ( $V_x$ ). But in Simulink, it is necessary to calculate the load torque ( $T_L$ ). Hence, the vehicle speed ( $V_x$ ) is translated again into a loading torque using Eq. (17) considering wheel radius. Instead of those complications, a passive loading scheme can be used for the EV [36]. The steady-state torque-speed characteristics of the EV can be obtained from Eq. (18). First, different torque values ( $T_e$ ) are applied. Then, the steady-state vehicle speed is reported for each torque value. At the end, full torque-speed characteristics for the EV can be obtained as shown in Fig. 3. These characteristics are used as a direct loading

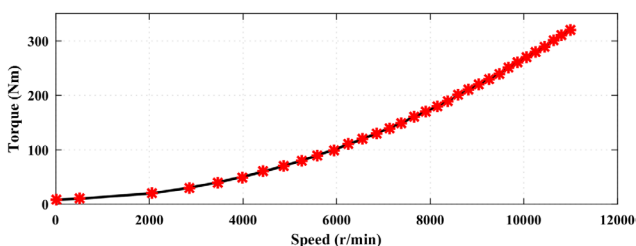


Fig. 3 Speed and torque profiles of the vehicle

torque for the IPMSM. The input is the vehicle speed and the output is the load torque ( $T_L$ ). It should be noted that the passive loading does not consider vehicle inertia. Hence, it should be included with the motor inertia. The specification of the electric vehicle are equivalent to Nissan Leaf 2018 electric car. They are given in Table 1.

#### 2.4 Estimation and modeling of inverter losses

In general, the inverter losses are categorized as the conduction losses and the switching losses. There is also the blocking loss. It can be neglected as it is a very small amount [37, 38]. The IGBT models that are used in this paper are 6MBI300V-120-50 from Fuji Electric Corp. The required IGBT data can be obtained from its online datasheet.

##### 2.4.1 Estimation of conduction losses

The conduction losses are like the resistive losses. It occurs when the IGBTs/diodes are conducting currents due to their internal resistances. These losses depend on current level and the junction temperature. The conduction losses of one IGBT ( $P_{C-IGBT}$ ) and the conduction loss for one diode ( $PC_{-diode}$ ) in a 2-level VSI can be defined as in Eq. (19) and Eq. (20), respectively [37].

$$P_{C-IGBT} = \frac{1}{T} \int_0^T (V_{ce}(t) \times I_{ce}(t)) dt, \quad (19)$$

Table 1 The vehicle parameters

Geometry parameter	Value
Peak output power	110 kW
Maximum speed	200 km/h
Rated torque	160 Nm
Drag coefficient ( $C_d$ )	0.28
Frontal area ( $A_f$ )	2.3 m <sup>2</sup>
Rolling resistance ( $f_r$ )	0.01
Dynamic tire radius ( $R_w$ )	0.6324 m

$$P_{C-diode} = \frac{1}{T} \int_0^T (V_F(t) \times I_F(t)) dt, \quad (20)$$

where  $V_{ce}$  is the collector-emitter voltage,  $I_{ce}$  is the IGBT collector current,  $V_F$  is the diode forward voltage, and  $I_F$  is the diode forward current.

The voltages  $V_{ce}$  and  $V_F$  vary with current. In this paper, fitting is done to estimate the voltages ( $V_{ce}$  and  $V_F$ ) from the instantaneous currents ( $I_{ce}$  and  $I_F$ ) in both IGBTs and diodes. The data are obtained directly for the manufacturer datasheets as seen in Fig. 4. Due to the symmetrical load of the inverter as it is a 3-phase motor, the total conduction losses of the inverter can be estimated by multiplying Eqs. (19), (20) with a factor of 6.

### 2.4.2 Estimation of switching losses

The switching losses are the needed amount of energy to on or off any electronic switch. It is a small amount of energy but due to the huge number of on and off times per second, the total dissipated energy cannot be ignored. The switching losses occur in both IGBTs and diodes. These losses depend on the switching frequency, junction temperature, dc link voltage, and the current level.

The manufacturer datasheets mostly include the conduction losses against current for a reference voltage level. For accurate estimation of the switching losses, their values have to be estimated according to the current level and dc voltage magnitude. There is a linear relationship between these losses and the voltage [39]. Hence, the calculation accuracy depends mainly on the estimation of these losses according to current level. These can be easily achieved

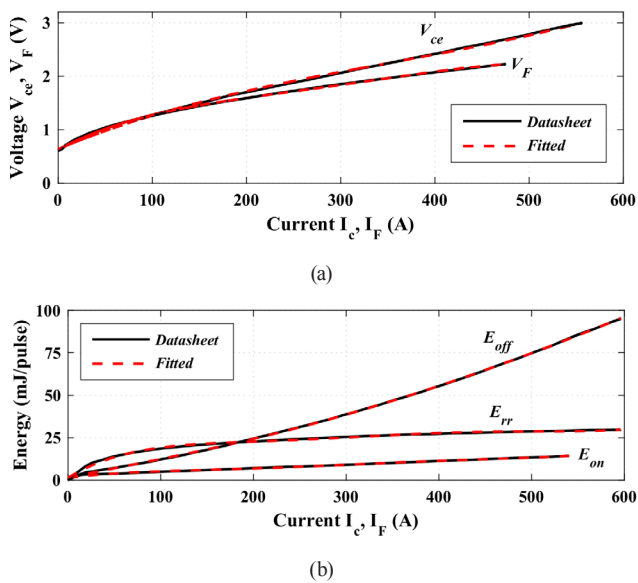


Fig. 4 Curve fitting of IGBT data (a) fitting of  $V_{ce}$  and  $V_F$ , (b) fitting of  $e_{on}$ ,  $e_{off}$ , and  $e_{rr}$

by direct fitting for the given data in manufacturer datasheets. The fitting of these values with simple polynomial function is shown in Fig. 4(b). This figure fits the dissipated energy during the switching-on ( $e_{on}$ ), switching-off ( $e_{off}$ ), and diode reverse recovery ( $e_{rr}$ ). Hence, the switching losses of one IGBT ( $P_{SW-IGBT}$ ) and the switching loss for one diode ( $P_{SW-diode}$ ) in a 2-level VSI can be defined as in Eqs. (21), (22), respectively [39].

$$P_{SW-IGBT} = (e_{on}(t) + e_{off}(t)) f_s \left( \frac{V_{dc}}{V_{nom}} \right), \quad (21)$$

$$P_{SW-diode} = e_{rr}(t) f_s \left( \frac{V_{dc}}{V_{nom}} \right), \quad (22)$$

where  $V_{nom}$  is the test voltage in datasheets. The total switching losses of the inverter can be estimated by multiplying Eqs. (21), (22) by a factor of 6. An overview of the inverter conduction and switching power loss is shown in Fig. 5(a, b), respectively.

### 2.5 Performance indices

The performance indices includes the online calculation of torque and flux ripples, the mechanical output power ( $P_m$ ), the total harmonic distortion (THD) of phase current, the switching frequency of inverter ( $f_{sw}$ ), the inverter losses ( $P_{inv}$ ), and the total efficiency ( $\eta_{total}$ ).

The standard deviation of ripples over one electric cycle ( $\tau$ ) is used to evaluate the torque-ripple ( $T_{rip}$ ) and the flux-ripple ( $\lambda_{rip}$ ) as follows in Eqs. (23) and (24) [19, 22]:

$$T_{rip} = \sqrt{\frac{1}{\tau} \int_0^\tau (T_e(t) - T_{ref}(t))^2 dt}, \quad (23)$$

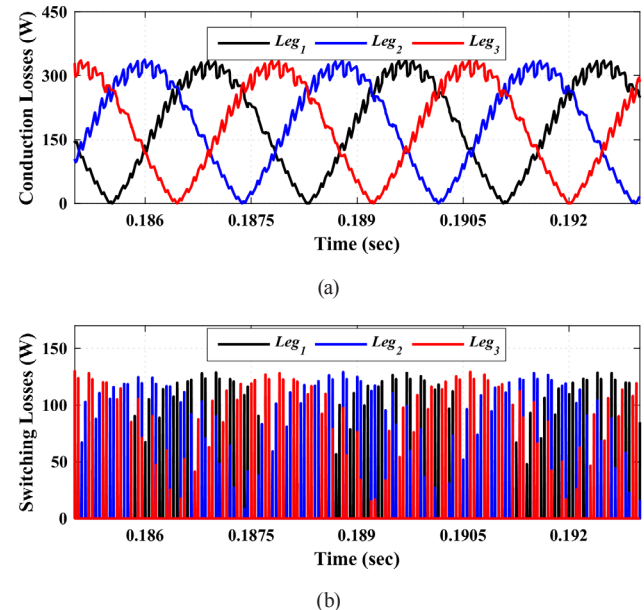


Fig. 5 The inverter losses (a) the conduction losses; (b) the switching losses

$$\lambda_{rip} = \sqrt{\frac{1}{\tau} \int_0^\tau (\lambda_s(t) - \lambda_{ref}(t))^2 dt}. \quad (24)$$

The mechanical output power can be estimated from motor speed ( $\omega$ ) as follows in Eq. (25):

$$P_m = T_{av}(t) \cdot \omega(t), \quad (25)$$

where  $T_{av}$  is the average motor torque.

Eq. (26) is the most adopted for spectrum performance for THD of stator current [22].

$$\text{THD} = \sqrt{\frac{I_{rms}^2 - I_{1,rms}^2}{I_{1,rms}^2}}, \quad (26)$$

where  $I_{1,rms}$  represents the root mean square (RMS) value of fundamental component of stator current.  $I_{rms}$  depicts the RMS value of stator current.

The switching frequency of inverter is calculated as in Eq. (27):

$$f_{sw} = \frac{1}{\tau} \int_0^\tau N_T dt, \quad (27)$$

where  $N_T$  is the total number of switchings for the VSI over one electric period  $\tau$ .

The total system efficiency ( $\eta_{total}$ ) is calculated based on losses and mechanical power as in Eq. (28):

$$\eta_{total} = \frac{P_m}{P_m + P_{cu} + P_{Fe} + P_{inv}} \times 100. \quad (28)$$

### 3 Reference flux calculation for MTPA

The MTPA is achieved based on the minimization of copper loss. The idea is to have the minimum armature current ( $I_a$ ) with constant torque [40]. If  $i_x$  and  $i_y$  are the  $x$  and  $y$ -axis components of  $I_a$ , then the MTPA can be developed such as derivative of  $I_a$  in Eq. (29) for a variable  $h$  goes to zero.

$$I_a^2 = I_x^2 + I_y^2, \quad (29)$$

$$\frac{\partial}{\partial h} I_x^2 + \frac{\partial}{\partial h} I_y^2 = 0, \quad (30)$$

by solving Eq. (30) in the  $d$ - $q$  frame, the following relationship between  $i_d$  and  $i_q$  in MTPA condition is obtained. In this case, the variable  $h$  should be the stator flux ( $\lambda_s$ ) [11, 41].

$$i_d = \frac{\lambda_{pm}}{2(L_q - L_d)} - \sqrt{i_q^2 + \frac{\lambda_{pm}^2}{4(L_q - L_d)^2}}. \quad (31)$$

In IPMSMs,  $L_d$  is bigger than  $L_q$ . Hence,  $i_d$  cannot be positive. Hence, the relationship can be expressed as:

$$(L_q - L_d)^2 i_q^2 = \lambda_b (\lambda_b - \lambda_{pm}), \quad (32)$$

where:

$$\lambda_b = \lambda_{pm} - (L_q - L_d) i_d. \quad (33)$$

In IPMSM,  $i_d$  is less than zero ( $i_d < 0$ ) and  $L_q$  is greater than  $L_d$  ( $L_q > L_d$ ). Hence,  $\lambda_b$  will be greater than  $\lambda_{pm}$  ( $\lambda_b > \lambda_{pm}$ ). The stator flux  $\lambda_s$  can be written as:

$$\lambda_s^2 = (\lambda_{pm} + L_d i_d)^2 + (L_q i_q)^2, \quad (34)$$

by substituting Eq. (32) and Eq. (33) into Eq. (6) and Eq. (34),  $T_e$  and  $\lambda_s$  can be represents as functions of  $\lambda_b$  as follows in Eqs. (35) and (36):

$$\left( \frac{L_q - L_d}{P} T_e \right)^2 = (\lambda_b - \lambda_{pm}) \lambda_b^3, \quad (35)$$

$$\begin{aligned} \lambda_{s\_MTPA}^2 &= \frac{(L_q^2 + L_d^2) \lambda_b^2 - L_q (L_q + 2L_d) \lambda_b \lambda_{pm} + L_q^2 \lambda_{pm}^2}{(L_q - L_d)^2}, \end{aligned} \quad (36)$$

where  $\lambda_{s\_MTPA}$  is the stator flux that fulfills MTPA conditions and satisfies Eq. (31).

Equations (35) and (36) are also described as follows in Eqs. (37) and (38):

$$\left( \frac{L_q - L_d}{p \lambda_{pm}^2} T_e \right)^2 = (Y - 1) Y^3, \quad (37)$$

$$\begin{aligned} \lambda_{s\_MTPA}^2 &= \frac{(L_q^2 + L_d^2) Y^2 - L_q (L_q + 2L_d) Y + L_q^2}{(L_q - L_d)^2} \lambda_{pm}^2, \end{aligned} \quad (38)$$

where  $Y$  is defined as:

$$Y = \frac{\lambda_b}{\lambda_{pm}}. \quad (39)$$

Equation (37) is a quartic-equation for  $Y$ . It has four solutions as follows in Eqs. (40) and (41) [41]:

$$Y = \frac{(B+1)}{4} \left( 1 \pm \sqrt{\frac{2}{B}-1} \right), \quad (40)$$

$$Y = \frac{(B-1)}{4} \left( 1 \pm \sqrt{-\frac{2}{B}-1} \right), \quad (41)$$

where:

$$B = \sqrt{\frac{1}{2} \left\{ \left( \sqrt{3X^2 + 1} + 1 \right)^{\frac{1}{3}} - \left( \sqrt{3X^2 + 1} - 1 \right)^{\frac{1}{3}} \right\}^3}, \quad (42)$$

$$X = \frac{16(L_q - L_d)}{9p\lambda_{pm}^2} T_{ref}. \quad (43)$$

$B$  and  $X$  are also non-dimensional variables.

The solution of Eq. (37) is limited only to Eq. (44) because  $Y$  must not be negative.

$$Y = \frac{(1+B)}{4} \left( 1 + \sqrt{\frac{2}{B} - 1} \right). \quad (44)$$

Fig. 6 shows the calculation procedure of  $\lambda_{s-MTPA}$ . First,  $Y$  is computed from  $T_{ref}$  using Eqs. (42) to (44). Then,  $\lambda_{s-MTPA}$  is determined from  $Y$  using Eq. (38). After that,  $\lambda_{s-MTPA}$  is applied to  $\lambda_{ref}$ . The parameter variations can be easily applied to Eqs. (38) and (43).

The reference d-and q-axis currents  $i_{d-ref}$  and  $i_{q-ref}$  can be described by Eqs. (45), (46), respectively:

$$i_{d-ref} = \frac{\lambda_{pm}}{(L_d - L_q)} (Y - 1), \quad (45)$$

$$i_{q-ref} = \frac{T_{ref}}{p\lambda_{pm} Y}. \quad (46)$$

#### 4 Basic traction drive topologies for EVs

For EVs, the operating point is changing consistently. If the rated dc voltage is applied at low speeds, the harmonic content of stator current will be high. On the contrary, lower voltages at low speed not only reduce the THD of stator current but also improve the overall drive performance. They contribute to achieving higher efficiency values as the inverter losses are reduced [2, 7].

Fig. 7 gives the basic traction topology for EVs. The inverter is combined with a boost converter that controls the dc voltage according to motor speed. The system voltage is controlled in a proportional way to the back-emf of IPMSM. The system voltage profile is illustrated in Fig. 8. At low speed, the inverter voltage will be the lowest available voltage that is the battery voltage. As the motor accelerates, the inverter voltage is increased

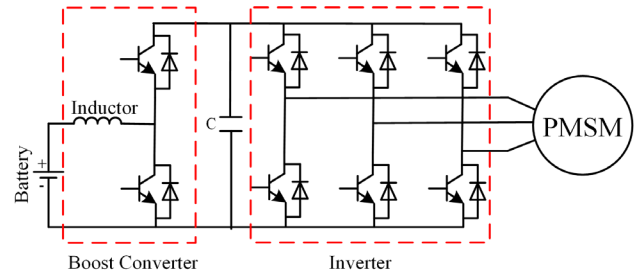


Fig. 7 Basic traction electric drive topologies for electric/hybrid vehicles

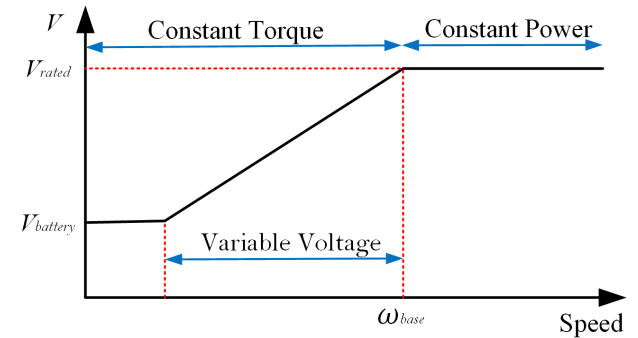


Fig. 8 Required system voltage with variable-voltage control

proportionally with the motor speed or back-emf voltage. Above base speed, in constant power region, the inverter is supplied with the rated motor voltage. Further improvements of overall system performance can be achieved, if the system voltage considers also the load level.

#### 5 Speed control based fuzzy logic controller

The fixed-gain PI controllers are commonly used in industrial applications. The fixed value of gains may provide reasonable performance under certain operating condition, but it has performance degradation for the other operating conditions. Besides, the gains are usually estimated using time-consuming trial-and-error methods. On the other hand, the FLC is a rule-based non-linear controller, it has no mathematical modeling. FLCs are more robust against the variation of plant parameter, they also have a better noise rejection capabilities [42, 43].

Fig. 9 illustrates the schematic of FLC that has two inputs and one output. The inputs are the speed error ( $e$ ) and its derivative ( $\Delta e$ ). The output is the reference torque.

The proposed system considers 7\*7 triangular membership functions (MFs) for inputs and output variables. The values of MFs are set by the hit and trial method. The 7\*7

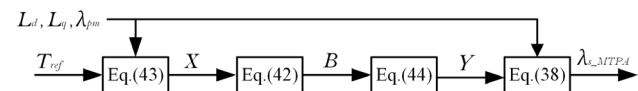


Fig. 6 Block diagram of the direct calculation of reference flux-linkage for MTPA control

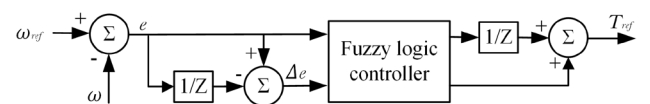


Fig. 9 Schematic model of fuzzy logic controller

MFs of inputs and output are shown in Fig. 10. The rules of FLC are set according to Table 2.

### 6 Field oriented control (FOC) technique

Fig. 11 illustrates the block diagram of FOC technique. It is implemented in the rotor flux reference frame using two PI current controllers and a fuzzy logic speed controller. The MTPA provides the reference d and q-axis currents. For fast dynamics, decoupling circuit is employed. Therefore, the PMSM seems a linear system to the current controllers as its non-linear part has been removed. A space vector pulse width modulator (SVPWM) is utilized to generate the desired voltage vector [2].

### 7 Direct torque control (DTC)

Fig. 12 shows the block diagram of DTC scheme. It involves a switching table, hysteresis controllers, and torque and flux estimators. The torque and flux are estimated based

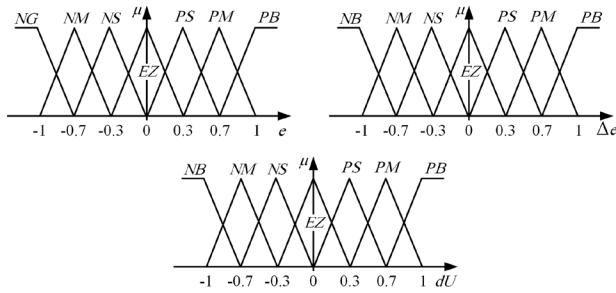


Fig. 10 The fuzzy membership functions

Table 2 The fuzzy logic control rules

		$\Delta e$						
		NB	NM	NS	EZ	PS	PM	PB
$e$	NB	NB	NB	NB	NB	NM	NS	EZ
	NM	NB	NB	NB	NM	NS	EZ	PS
	NS	NB	NB	NM	NS	EZ	PS	PM
	EZ	NB	NM	NS	EZ	PS	PM	PB
	PS	NM	NS	EZ	PS	PM	PB	PB
	PM	NS	EZ	PS	PM	PB	PB	PB
	PB	EZ	PS	PM	PB	PB	PB	PB

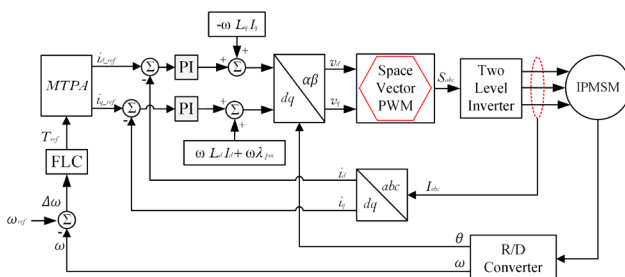


Fig. 11 The system configuration of field-oriented PMSM

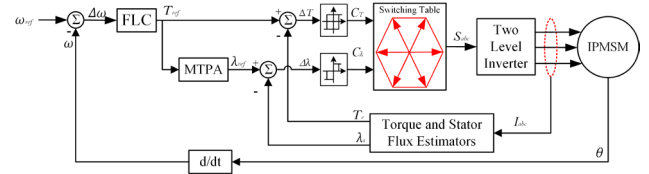


Fig. 12 The schematic diagram of conventional DTC

on machine model. They are used directly as feedback signals. The hysteresis controllers are used for both the torque and flux. They are employed to quantize the torque and flux errors ( $\Delta T$  and  $\Delta \lambda$ ) into integer outputs ( $C_T$  and  $C_\lambda$ ). The optimal voltage vector is selected according to sector number,  $C_T$  and  $C_\lambda$ . The selection of voltage vector is done according to the switching table (Table 3). After the selection of voltage vector, it is applied to the VSI to minimize torque and flux errors [13].

The available voltage vectors for two-level VSI are only eight vectors. They are shown in Fig. 13 in the  $\alpha\beta$  stationary reference frame. As noted, there are 6 active vectors ( $V_1$  to  $V_6$ ). The vectors  $V_0$  and  $V_7$  are zero vectors. In each sector there is a group of vectors that can increase/decrease the flux and torque. The optimal voltage vector according to each sectors are included in Table 3. For example in sector 1, the selection of  $V_2$  and  $V_6$  increases the flux;  $V_3$  and  $V_5$  decreases the flux;  $V_2$  and  $V_3$  increase the torque angle and hence the torque itself;  $V_5$  and  $V_6$  decreases the torque.  $V_0$  and  $V_7$  decrease the torque and maintain constant flux. Therefore, if the torque and flux are required to increase,  $V_2$  is the required vector.

### 8 Model predictive control

Fig. 14 gives the block diagram for the finite set model predictive direct torque control (FS-MPDTC). The MPDTC uses machine model to predict its future trajectory states. The control algorithm predicts the motor state for the eight available voltage vectors of VSI using the discrete model of the drive. Using the Forward Euler approximation, the discrete model of IPMSM is set as follows in Eqs. (47) and (48) [20, 22]:

Table 3 The Voltage Vector LUT of DTC

$C_\lambda$	$C_T$	$Sec_1$	$Sec_2$	$Sec_3$	$Sec_4$	$Sec_5$	$Sec_6$
1		$V_2$	$V_3$	$V_4$	$V_5$	$V_6$	$V_1$
		$V_7$	$V_0$	$V_7$	$V_0$	$V_7$	$V_0$
		$V_6$	$V_1$	$V_2$	$V_3$	$V_4$	$V_5$
		$V_3$	$V_4$	$V_5$	$V_6$	$V_1$	$V_2$
0		$V_0$	$V_7$	$V_0$	$V_7$	$V_0$	$V_7$
		$V_5$	$V_6$	$V_1$	$V_2$	$V_3$	$V_4$



**Table 4** The major parameters of IPMSM [2]

Parameter	Value
No. of poles	8
Power (max)	100 Kw
Max. torque (60 sec)	320 Nm
Max. current	293 Arms
Rated torque ( $\geq 30$ min)	160 Nm
Rated current	150 Arms
DC link voltage	260 ~ 360 V
Base speed	3600 rpm
Max. speed	12000 rpm
Inductance ( $L_d/L_q$ )	0.234/0.562 mH
Coil resistance ( $R_s$ )	13 m $\Omega$
PM flux ( $\lambda_{pm}$ )	0.0927 Wb
The simulation step time	1 $\mu$ s
Control period	50 $\mu$ s

### 9.1 Dynamic behavior under EV loading

The comparative study between DTC, MPDTC and FOC is done for the following perspectives: torque and flux ripples, inverter frequency, inverter losses, iron losses, copper losses, mechanical output power, total efficiency, and THD of stator current. The simulation results are shown in Figs. 15–20.

The vehicle speed, motor speed, torque, and flux curves are given in Fig. 15. The reference vehicle speed is changed suddenly from 75 km/h to 150 km/h at 0.5 sec, then to 230 km/h at 1.0 sec as seen in Fig. 15(a). The corresponding motor speeds are shown in Fig. 15(b). For the three control strategies, the motor has a good speed tracking capability but with different responses. Both MPDTC and FOC reach the desired speed faster than DTC till speed of 4000 r/min, after that the FOC shows a slower acceleration performance. As the motor accelerates the load torque of EV increases as shown in Fig. 15(c). Hence, the vehicle reaches a steady state speed of about 220 km/h. Noting that the maximum vehicle speed is 200 km/h.

The torque of FOC shows an overshoot which depends on the control parameters as illustrated in Fig. 15(d). The reason why DTC shows a slow acceleration is that its mean torque is smaller compared to MPDTC and FOC. The flux curves in Fig. 15(e) are estimated for MTPA till rated speed then for field weakening till maximum possible speed. For speed higher than the rated motor speed (3600 r/min), field weakening is must for motor operation as seen in Fig. 15(e) after 1.0 sec. as noted, the MPDTC shows the best performance in field weakening region, followed by DTC, then FOC.

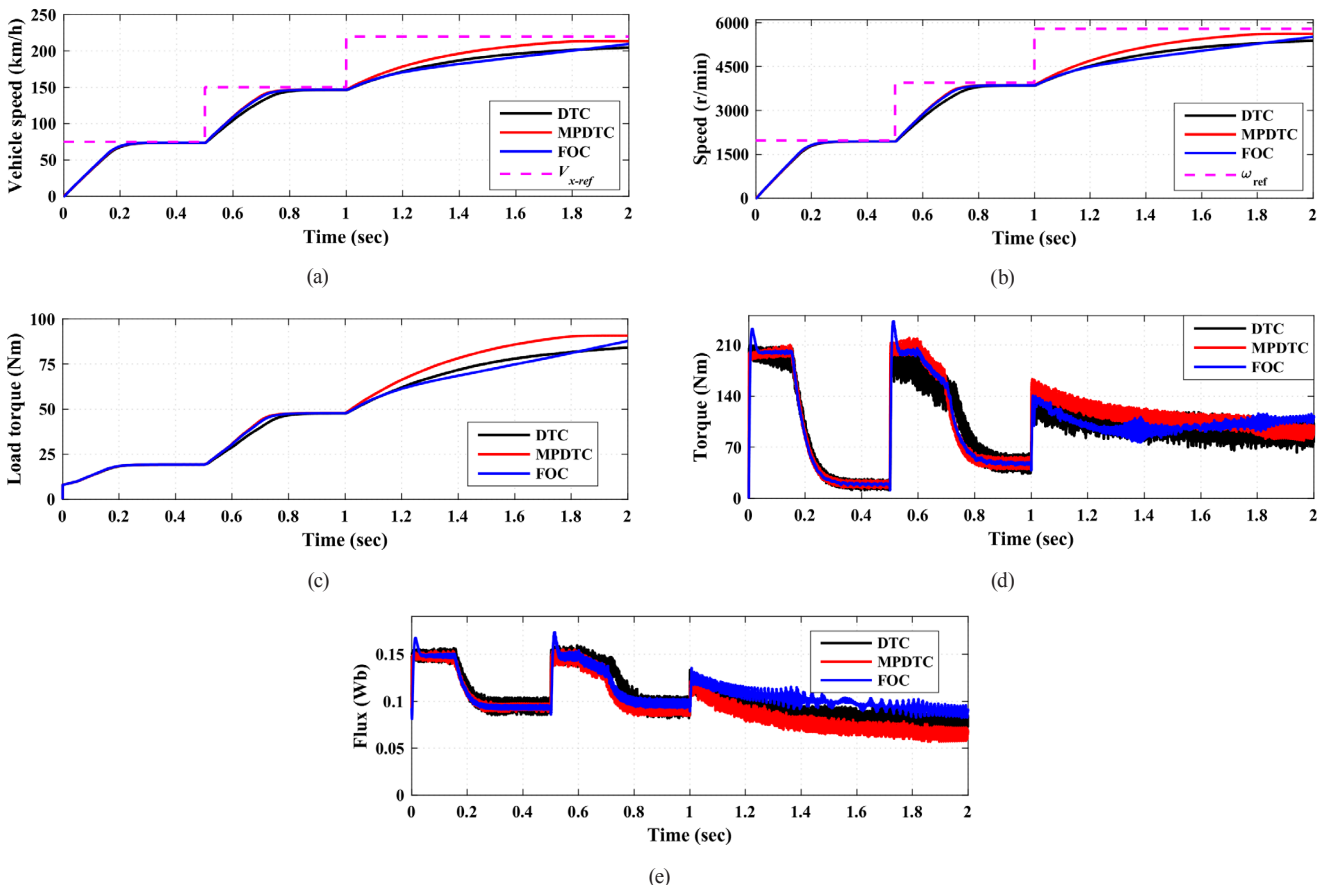


**Fig. 15** The simulation results under dynamic state. (a) vehicle speed, (b) motor speed, (c) load torque, (d) torque, (e) flux-linkage

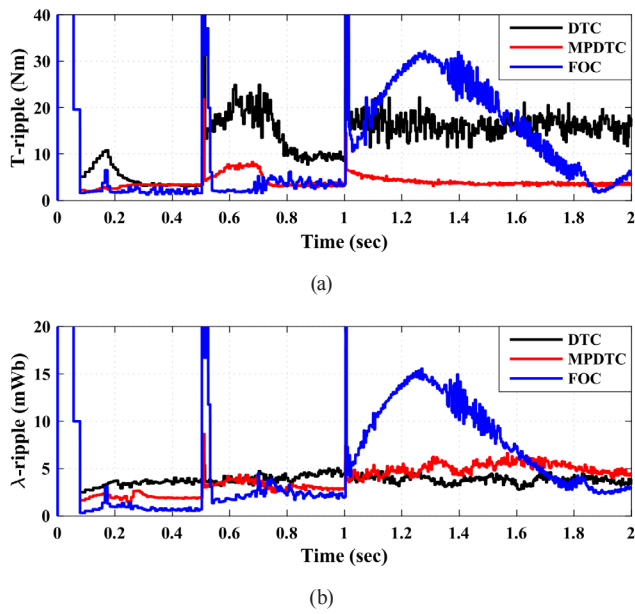


Fig. 16 The torque and flux ripples (a) torque ripples, (b) flux ripples

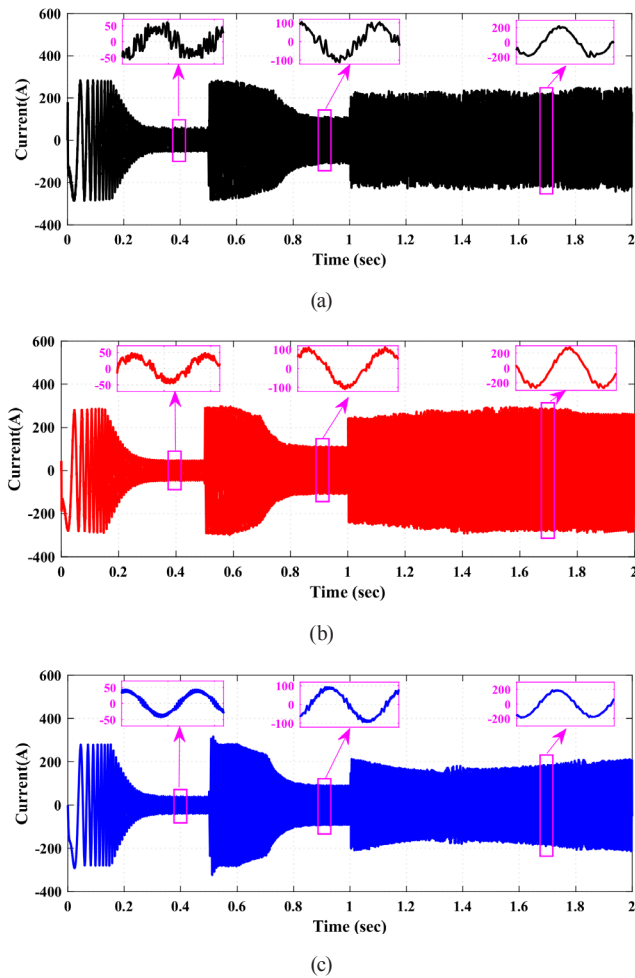


Fig. 17 The phase current waveform (a) DTC, (b) MPDTC, (c) FOC

### 9.1.1 The torque and flux ripples

The torque and flux profiles that are seen in Fig. 15(d, e) give a perspective view of the ripples. The online torque

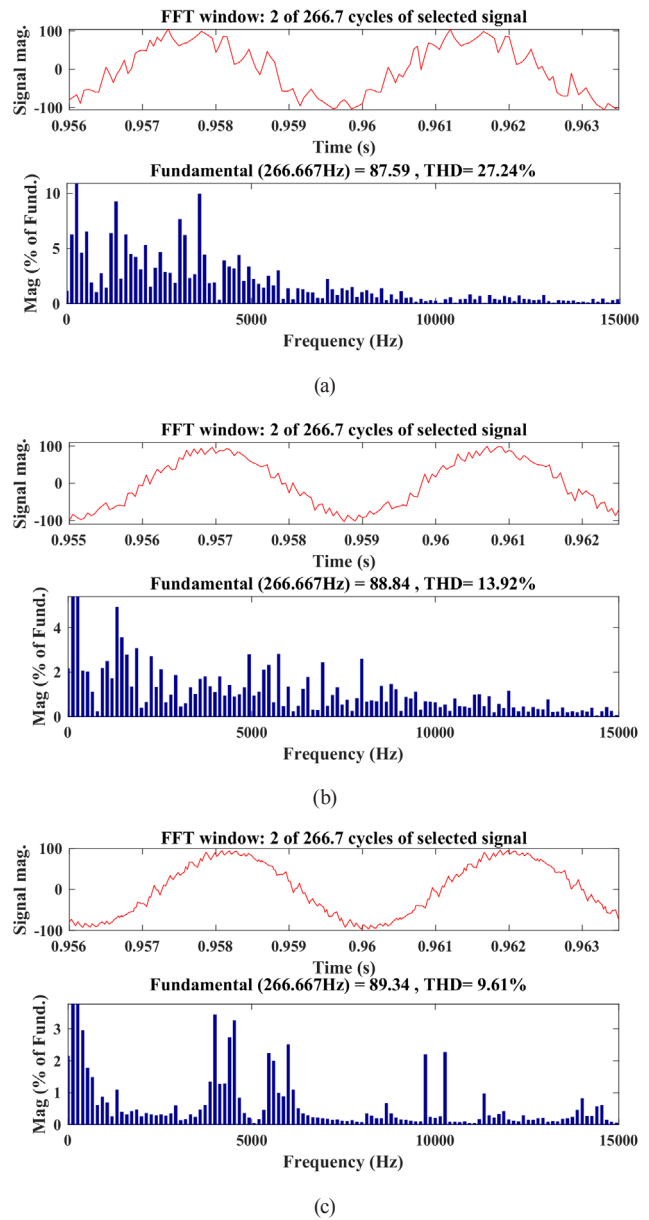


Fig. 18 FFT of phase current (a) DTC, (b) MPDTC, (c) FOC

and flux ripples are shown in Fig. 16(a, b), respectively. As noted, under MTPA operation (till rated speed), the FOC has the smoothest torque and flux profiles. Hence, the lowest torque and flux ripples. The MPDTC shows a very similar performance to FOC. On the contrast, the DTC shows the poorest performance. In the field weakening zone (after 1.0 sec), the MPDTC shows the best overall performance of torque ripple, followed by DTC, then FOC. However, the FOC has a smooth torque profile (see Fig. 15(d)), it does not track properly the commanded reference torque, hence, it shows high torque and flux ripples.

It can be concluded that, the FOC shows the lowest torque and flux ripples under MTPA operation (till rated speed), and the MPDTC shows the best performance under field weakening operation

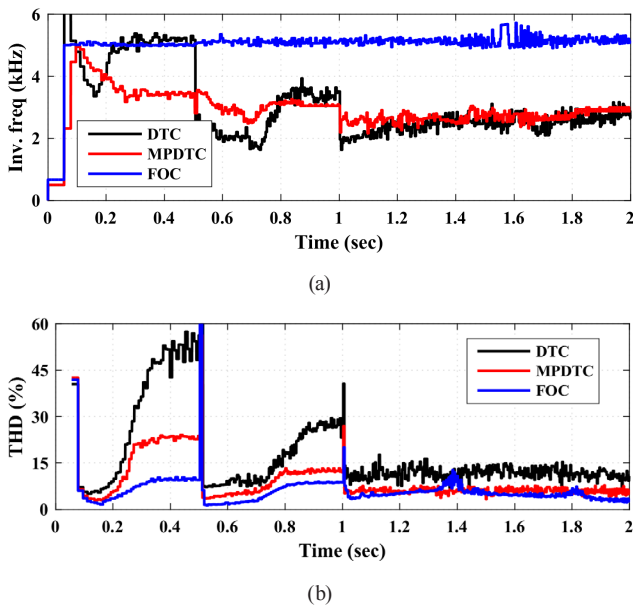


Fig. 19 The inverter frequency and THD. (a) frequency, (b) THD

### 9.1.2 The inverter frequency and THD of stator current

One phase current for each control strategy is shown in Fig. 17(a–c). The motor current is dynamically adjusted according to the load torque and speed. The MPDTC has the fastest current response as seen on its profile in Fig. 17(b) compared to the one of DTC in Fig. 17(a) and that of FOC in Fig. 17(c).

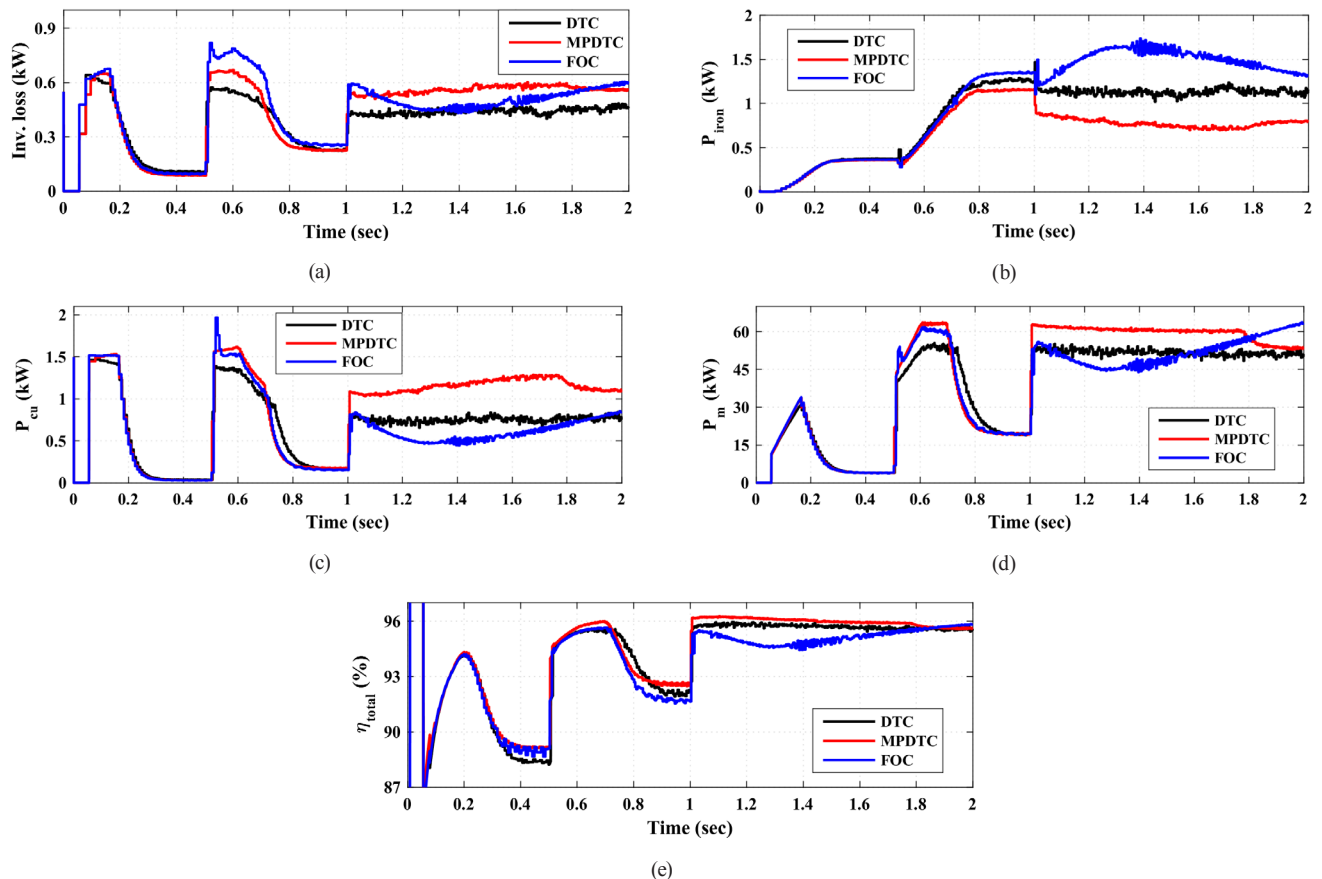


Fig. 20 The losses and efficiency curves (a) inverter losses, (b) iron losses, (c) copper losses, (d) mechanical power, (e) total efficiency

The harmonic content in phase currents can be clearly noticed over the zooming parts of current curves in steady state. As noted, the DTC has the highest harmonic content in current waveform. On the other side, the FOC has the lowest harmonic content in stator current.

The stator phase current waveforms with fast Fourier transform (FFT) and THD calculation for the different control strategies are illustrated in Fig. 18(a–c). The calculation process includes 2 cycles of phase current. The results are obtained under steady state condition (4000 r/min). As noted, the biggest distortion of current waveforms and the highest THD are held by DTC. The performance of FOC and MPDTC is superior to that of DTC, especially FOC as it has few high-frequency harmonics.

The inverter frequency and the THD are seen in Fig. 19 (a, b), respectively. As noted, the FOC has a fixed switching frequency. On the contrary, the DTC and MPDTC posse variable switching frequencies. The MPDTC has a lower switching frequency compared to DTC thanks to the dynamic cost function.

The FOC has the lowest THD while The DTC has the highest THD over the entire speed range. The MPDTC comes in the middle range but closer to FOC. Under high speeds, the MPDTC provides shows a similar value of THD as in FOC.

### 9.1.3 Losses and efficiency

The losses and efficiency curves are as shown in Fig. 20. The inverter losses depend basically on the switching frequency of inverter and the current level. The higher switching frequency is translated into higher inverter losses that are seen in Fig. 20(a).

In general, the MPDTC has the lower switching frequency and hence the lower inverter losses under MTPA operation, then it shows the highest inverter losses. From 0.5 sec to 0.7 sec, the DTC possess the lowest inverter losses as it has a lower mean torque and hence smaller current level. After 1.0 sec, the DTC has the same switching frequency as MPDTC but with lower loading torque, hence, it shows the lowest inverter losses.

As shown in Fig. 20(b), the MPDTC exhibits low iron losses. But it has higher copper losses compared to DTC and FOC especially under high speeds as shown in Fig. 20(c). The higher copper losses return to the fact that MPDTC has the capability to draw much current from supply. This current is converted to a useful mechanical output power as illustrated in Fig. 20(d). For the DTC, the output power on the same period is smaller as it has a lower average torque production. The efficiency curves are seen in Fig. 20(e). The MPDTC provides the higher total efficiency.

As concluded, The MPDTC can draw more current (that means more copper losses); it also converts the current into a useful mechanical output power with higher conversion efficiency compared to DTC and even FOC.

### 9.1.4 Stator flux loci

The flux locus is shown in Fig. 21. The three control strategies have a constant flux magnitude that is represented by a circle. Fig. 21 (a) shows the flux locus under steady

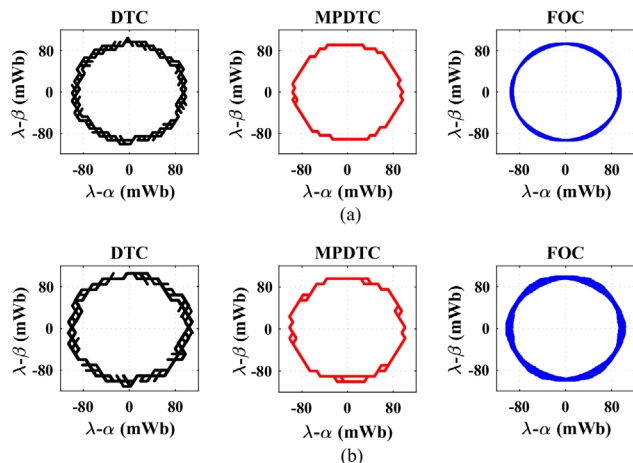


Fig. 21 The stator flux loci in steady-state, (a) at 2000 r/min (0.3 – 0.5 sec); (b) at 4000 r/min (0.8 - 1 sec)

state speed of 2000 r/min. It is noted that, for low speeds, the FOC has the best shape with smoother stator flux locus followed by MPDTC then DTC. The MPDTC has a more circular shape for its stator flux locus than DTC.

Fig. 21(b) shows the flux locus under steady state speed of 4000 r/min. as noted, the performance of FOC is deteriorated in smoothness and stator flux ripples compared to that at 2000 r/min (Fig. 21(a)). On the other hand, for both DTC and MPDTC, the stator flux loci don't have a significant change in the shape and smoothness compared to their performances at 2000 r/min.

As a conclusion, for all investigated control strategies, the performance of stator flux loci deteriorates in both shape and smoothness with increasing the motor speed. Besides, the performance also deteriorates with increasing the load torque for all control strategies.

### 9.1.5 Dynamic torque response

The dynamic torque response to a step-change of reference torque is shown in Fig. 22. The results are obtained for DTC, MPDTC, FOC-1, and FOC-2. The difference between FOC-1 and FOC-2 is the gains of PI current controllers. For MPDTC, it requires less than 1.14 msec for motor torque to reach it reference ( $T_{ref}$ ). This time is taken as the base response (100 %) as given in Table 5. The MPDTC has the fastest torque response, followed by DTC, then FOC-2, and then FOC-1. It can be proclaimed that the fast dynamics of DTC is also maintained in MPDTC with an improved steady-state performance. For FOC, the dynamic torque response depends basically on the tuning of its PI gains. The FOC-2 can provide a quick response, but undesirable overshooting is noticed. If the PI gains are tuned to eliminate the overshooting, a lengthened response time is observed as seen for FOC-1. The relative time responses and overshoot results are given numerically in Table 5.

### 9.2 The steady-state performance under the same frequency

To fairly evaluate the performance of control strategies, a comparison under the same switching frequency of inverter

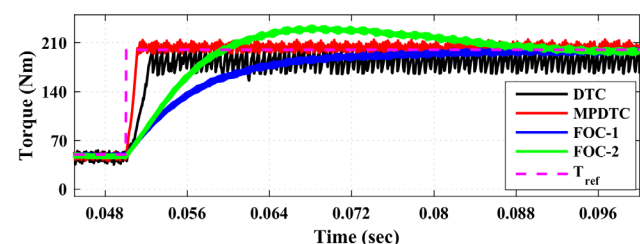


Fig. 22 The torque response

**Table 5** The numeric analysis of torque response

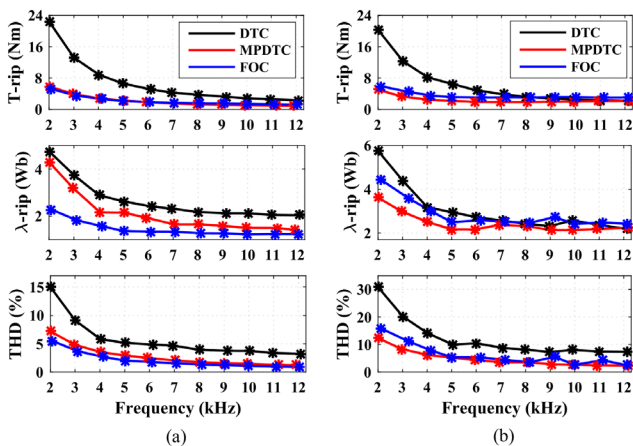
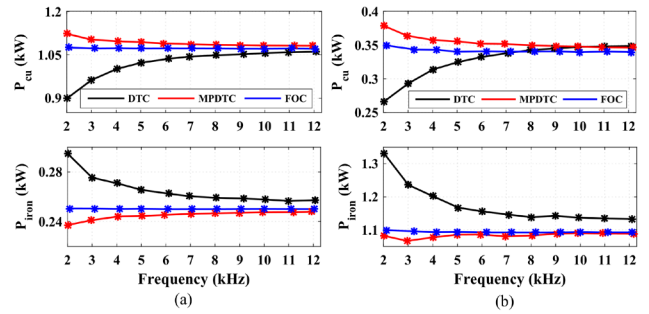
Parameter	MPDTC	DTC	FOC-2	FOC-1
Time to reach $T_{ref}$ (sec)	0.00114	0.00257	0.00958	0.04908
Time response (%)	100	44.36	11.89	2.32
Overshot (%)			17.25	

is obtained. The comparison involves the torque ripples, flux ripples, and THD as shown in Fig. 23. Besides, it also includes the copper and iron losses as seen in Fig. 24. The frequency is changed from 2 kHz to 12 kHz. The results are obtained at speed of 1800 r/min with 160 Nm load torque and at speed of 3600 r/min with 80 Nm load torque.

In order to obtain the desired switching frequency for each control technique, different procedures are employed. In DTC, the hysteresis bounds for both the torque and flux in addition to the control period (sample time) are adjusted. For MPDTC, the control period and the coefficients  $w_\lambda$  and  $w_s$  are tuned. For FOC, the PWM frequency is set directly to the desired value.

As noted, different control performances for the control strategies are obvious under same switching frequency. In Fig. 23(a, b), the DTC features the biggest torque ripples, the highest flux ripples, and the most THD over the entire frequency band. The MPDTC and FOC feature lower torque ripples, flux ripples, and THD than that of DTC. There is no significant difference between MPDTC and FOC in torque ripples and THD especially at low speed of 1800 r/min. The flux ripple of MPDTC depends on the weights of cost function. MPDTC held higher flux ripples than FOC at low speeds but features lower values at higher speed of 3600 r/min.

In Fig. 24(a, b), the DTC features the lowest copper losses for low and high speeds but held the highest


**Fig. 23** The torque ripples, flux ripples, and THD for the same frequency at (a) 1800 r/min with 160 Nm; (b) 3600 r/min with 80 Nm

**Fig. 24** The copper and iron losses for the same frequency at (a) 1800 r/min with 160 Nm, (b) 3600 r/min with 80 Nm

iron losses. Its lower copper losses are mainly because it draws a lower RMS current with limited capability of producing a mechanical output power and average torque. The MPDTC has the best capability of producing mechanical output power. Hence, it can draw higher currents from supply that verifies the higher copper losses. On the contrary, it features the lowest iron losses. The FOC has a similar performance to MPDTC.

As a conclusion, the DTC presents the biggest torque ripple, flux ripples, and THD of all presented schemes over the entire band of frequency. The MPDTC provides the best performance in torque ripple, flux ripples, and THD at high speeds. It also gives a very similar performance to FOC at low speeds except for flux ripples. These ripples depend on the cost function, may be a dynamic cost function fulfill the best overall performance over the entire frequency band.

### 9.3 Parameter sensitivity

For IPMSM, the sensitive parameters involve the winding resistance and the inductances ( $L_d, L_q$ ). The temperature affects winding resistance while the saturation influences the inductance values ( $L_d, L_q$ ). The proper estimation of these parameters is of great significance in practical implementations as it directly affects the system performance.

The stator flux can be estimated using voltage model as in Eq. (58) or using current model as in Eq. (59). As noted, the flux estimation is affected by the variation of machine parameters.

$$\lambda_{s,dq} = \int (V_{s,dq} - R_s i_{s,dq}) dt \quad (58)$$

$$\lambda_{s,dq} = G i_{s,dq} - \lambda_{r,dq} \quad (59)$$

The flux estimation based on voltage model is affected by the variation of winding resistance. The variation of resistance will result in a flux error. The flux error can be ignored at high speeds as the voltage drop against resistance is very

small compared to the voltage drop across inductance. On the contrary, the flux error can be significant under low speeds because the stator resistance can vary considerably because of the temperature and motor speed variations. In case the estimated value of stator resistance is lower than the actual one, the actual torque and flux deviate from the desired values. Whereas a higher estimated value for resistance may cause unstable drive system.

The variation of stator inductance directly influences the estimated stator flux using current model. Under saturation conditions, the inductance is affected greatly; the inductance values decrease with increasing the current [19]. Hence, high performance often requires the online estimation of machine parameters (resistance and inductance).

It is very difficult to conduct closed-form analytical solutions for parameter sensitivity evaluation because of the nonlinear nature of the control strategies. Therefore, an intentionally error is introduced in the machine parameters in order to evaluate the system performance. Fig. 25 shows the motor torque and flux waveforms using current model-based estimator. The values of machine parameters used by the controllers differ from their actual values by  $\pm 50\%$ . From 0.04 to 0.06, the controller uses the actual values of stator resistance and inductance; hence, high tracking performance is observed. Next, from 0.06 to 0.08, the controller uses  $+50\%$  higher values for the stator resistance and inductance. In contrast, from 0.08 to 0.1, the controller uses  $-50\%$  less values for the stator resistance and inductance. As noted, the torque of both DTC and FOC is mostly unaffected by the variation of machine parameters. The dashed purple trace is the reference. On

the contrary, the torque ripples of MPDTC are more sensitive to parameter variations. The performance control of stator flux has significant deterioration for both DTC and FOC because the inductance is used for flux estimation. The performance of MPDTC is less affected.

For the three control strategies, based on current model, the DTC needs only the stator inductance to achieve the torque estimation and the stator flux. As the MPDTC uses a prediction model, it is affected by both the stator resistance and inductance. The FOC does not require any of the parameters for its control strategy. But for comparison, its torque and stator flux are estimated. However, the torque ripple of FOC is affected slightly by parameters variation. The reason is that the calculation of PI gains depends on resistance and inductance values. Hence, the performance of FOC is affected indirectly by the machine parameters despite FOC strategy does not employ them.

#### 9.4 Algorithm complexity

Due to the limited hardware capacity, the complexity of control algorithm becomes unavoidable issue. If the control algorithm is too complicated, it may become practically unfeasible as the required time in each control period surpasses the hardware capabilities. Increasing the control period is one solution but may lead to the deterioration of control performance. The feasible solution is to simplify the control algorithm without exceeding the calculation limits of controllers.

The DTC features the simplest structures; it demands the least amount of computation to estimate only the stator flux and torque. On the contrary, the MPDTC uses a prediction algorithm that depends on the available voltage vectors. Its computational complexity is correlated to the number of voltage vectors. This number depends on the inverter topology (multi-level or two-level). The computation complexities of involve calculating the duty ratio of different voltage vectors.

#### 9.5 Summary of the comparative evaluation

Table 6 gives the major comparison results for the evaluated control strategies.

### 10 Conclusions

This paper provides a detailed analysis and comparative study for the DTC, MPDTC and FOC techniques based on IPMSM for EVs. Each one of these three control strategies can achieve the vehicle requirements but with different dynamic and steady-state performances. The DTC

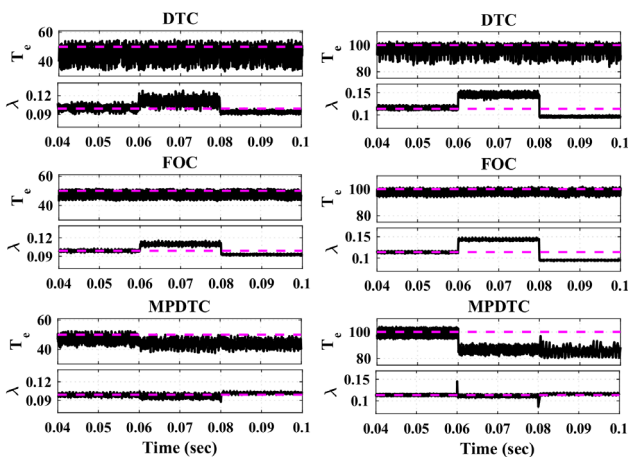


Fig. 25 The system performance with the variation of stator resistance and inductance by  $\pm 50\%$  of their actual at 3000 r/min. (a) 50 Nm load torque, 5 kHz; (b) 100Nm load torque, 7kHz. The dashed purple trace is the reference

**Table 6** Summary of comparison results

Geometry parameter	DTC	MPDTC	FOC
Torque ripple under same switching frequency	High	Middle	Low
Stator flux ripple	High	High	Low
Stator current THD	High	Middle	Low
Dynamic response	Fast	Fast	Slow
Machine losses	High	High	Low
Parameter sensitivity	Low	High	Low
Algorithm complexity	Low	High	Middle
Required control period	Short	Short	Long

features a fast-dynamic response with less algorithm complexity, but it has the highest torque ripples and the biggest THD for its stator current.

## References

- [1] Wu, J., Wang, J., Gan, C., Sun, Q., Kong, W. "Efficiency Optimization of PMSM Drives Using Field-Circuit Coupled FEM for EV/HEV Applications", *IEEE Access*, 6, pp. 15192–15201, 2018. <https://doi.org/10.1109/ACCESS.2018.2813987>
- [2] Nam, K. H. "AC Motor Control and Electrical Vehicle Applications", CRC Press, Boca Raton, FL, USA, 2019.
- [3] Ehsani, M., Gao, Y., Emadi, A. "Modern electric, hybrid electric, and fuel cell vehicles: fundamentals, theory, and design", CRC Press, Boca Raton, FL, USA, 2010.
- [4] Dang, L., Bernard, N., Bracikowski, N., Berthiau, G. "Design Optimization with Flux Weakening of High-Speed PMSM for Electrical Vehicle Considering the Driving Cycle", *IEEE Transactions on Industrial Electronics*, 64(12), pp. 9834–9843, 2017. <https://doi.org/10.1109/TIE.2017.2726962>
- [5] Zhang, Y., Cao, W., McLoone, S., Morrow, J. "Design and Flux-Weakening Control of an Interior Permanent Magnet Synchronous Motor for Electric Vehicles", *IEEE Transactions on Applied Superconductivity*, 26(7), pp. 1–6, 2016. <https://doi.org/10.1109/TASC.2016.2594863>
- [6] Parasiliti, F., Villani, M., Lucidi, S., Rinaldi, F. "Finite-Element-Based Multiobjective Design Optimization Procedure of Interior Permanent Magnet Synchronous Motors for Wide Constant-Power Region Operation", *IEEE Transactions on Industrial Electronics*, 59(6), pp. 2503–2514, 2012. <https://doi.org/10.1109/TIE.2011.2171174>
- [7] Estima, J. O., Marques Cardoso, A. J. "Efficiency Analysis of Drive Train Topologies Applied to Electric/Hybrid Vehicles", *IEEE Transactions on Vehicular Technology*, 61(3), pp. 1021–1031, 2012. <https://doi.org/10.1109/TVT.2012.2186993>
- [8] Huang, S., Wu, G., Rong, F., Zhang, C., Huang, S., Wu, Q. "Novel Predictive Stator Flux Control Techniques for PMSM Drives", *IEEE Transactions on Power Electronics*, 34(9), pp. 8916–8929, 2019. <https://doi.org/10.1109/TPEL.2018.2884984>
- [9] Li, G., Hu, J., Li, Y., Zhu, J. "An Improved Model Predictive Direct Torque Control Strategy for Reducing Harmonic Currents and Torque Ripples of Five-Phase Permanent Magnet Synchronous Motors", *IEEE Transactions on Industrial Electronics*, 66(8), pp. 5820–5829, 2019. <https://doi.org/10.1109/TIE.2018.2870359>
- [10] Morales-Caporal, R., Leal-López, M. E., Jesús Rangel-Magdaleno, J., de Sandre-Hernández, O., Cruz-Vega, I. "Direct torque control of a PMSM-drive for electric vehicle applications", In: 28th International Conference on Electronics, Communications and Computers (CONIELECOMP), Cholula, Mexico, 2018, pp. 232–237. <https://doi.org/10.1109/CONIELECOMP.2018.8327204>
- [11] Shinohara, A., Inoue, Y., Morimoto, S., Sanada, M. "Maximum Torque Per Ampere Control in Stator Flux Linkage Synchronous Frame for DTC-Based PMSM Drives Without Using q-Axis Inductance", *IEEE Transactions on Industrial Applications*, 53(4), pp. 3663–3671, 2017. <https://doi.org/10.1109/TIA.2017.2686800>
- [12] Zhang, Z., Wei, C., Qiao, W., Qu, L. "Adaptive Saturation Controller-Based Direct Torque Control for Permanent-Magnet Synchronous Machines", *IEEE Transactions on Power Electronics*, 31(10), pp. 7112–7122, 2016. <https://doi.org/10.1109/TPEL.2015.2511073>

The FOC feature the smoothest torque profile, it also has the lowest THD of stator current, but suffers from the lack of fast dynamic response as it employs PI controllers in the current control loop. Besides, it is sensitive to the variation of machine parameter indirectly. Moreover, it has a poor performance under field weakening operation.

The MPDTC feature a flexible control, as it has a cost function. Tradeoff between its weight factors can result in different performances. MPDTC features almost a similar performance that of FOC for both the torque ripples and THD under the same switching frequency. Besides, the better flexibility of MPDTC allows it to draw higher supply currents that are converted into a mechanical output power with higher conversion efficiency. Moreover, MPDTC has the fastest dynamic response. Furthermore, it shows the best performance under filed weakening operation. Therefore, the MPDTC is highly a powerful candidate for EV applications based IPMSMs.

- [13] Zhang, Z., Liu, X. "A Duty Ratio Control Strategy to Reduce Both Torque and Flux Ripples of DTC for Permanent Magnet Synchronous Machines", *IEEE Access*, 7, pp. 11820–11828, 2019. <https://doi.org/10.1109/ACCESS.2019.2892121>
- [14] Abassi, M., Khlaief, A., Saadaoui, O., Chaari, A., Boussak, M. "Performance analysis of FOC and DTC for PMSM drives using SVPWM technique", In: 16th International Conference on Sciences and Techniques of Automatic Control and Computer Engineering (STA), Monastir, Tunisia, 2015, pp. 228–233. <https://doi.org/10.1109/STA.2015.7505167>
- [15] Essalmi, A., Mahmoudi, H., Abbou, A., Bennassar, A., Zahraoui, Y. "DTC of PMSM based on artificial neural networks with regulation speed using the fuzzy logic controller", In: Proceedings of 2014 International Renewable and Sustainable Energy Conference (IRSEC), Ouarzazate, Morocco, 2014, pp. 879–883. <https://doi.org/10.1109/IRSEC.2014.7059801>
- [16] Korkmaz, F., Topaloğlu, İ., Çakir, M. F., Gürbüz, R. "Comparative performance evaluation of FOC and DTC controlled PMSM drives", In: 4th International Conference on Power Engineering, Energy and Electrical Drives, Istanbul, Turkey, 2013, pp. 705–708. <https://doi.org/10.1109/PowerEng.2013.6635696>
- [17] Martins, C. A., Roboam, X., Meynard, T. A., Carvalho, A. S. "Switching frequency imposition and ripple reduction in DTC drives by using a multilevel converter", *IEEE Transactions on Power Electronics*, 17(2), pp. 286–297, 2002. <https://doi.org/10.1109/63.988948>
- [18] Chen, M., Gao, H., Song, H. "Simulation study on a DTC system of PMSM", In: Proceedings of 2011 6th International Forum on Strategic Technology (IFOST), Harbin, China, 2011, pp. 564–569. <https://doi.org/10.1109/IFOST.2011.6021087>
- [19] Niu, F., Wang, B., Babel, A. S., Li, K., Strangas, E. G. "Comparative Evaluation of Direct Torque Control Strategies for Permanent Magnet Synchronous Machines", *IEEE Transactions on Power Electronics*, 31(2), pp. 1408–1424, 2016. <https://doi.org/10.1109/TPEL.2015.2421321>
- [20] Ban, F., Lian, G., Zhang, J., Chen, B., Gu, G. "Study on a Novel Predictive Torque Control Strategy Based on the Finite Control Set for PMSM", *IEEE Transactions on Applied Superconductivity*, 29(2), pp. 1–6, 2019. <https://doi.org/10.1109/TASC.2019.2890837>
- [21] Chen, Z., Tu, W., Yan, L., Luo, G. "Dynamic Cost Function Design of Finite-Control-Set Model Predictive Current Control for PMSM Drives", In: 2019 IEEE International Symposium on Predictive Control of Electrical Drives and Power Electronics (PRECEDE), Quanzhou, China, 2019. <https://doi.org/10.1109/PRECEDE.2019.8753287>
- [22] Sandre-Hernandez, O., Rangel-Magdaleno, J., Morales-Caporal, R. "A Comparison on Finite-Set Model Predictive Torque Control Schemes for PMSMs", *IEEE Transactions on Power Electronics*, 33(10), pp. 8838–8847, 2018. <https://doi.org/10.1109/TPEL.2017.2777973>
- [23] Liu, Q., Hameyer, K. "Torque Ripple Minimization for Direct Torque Control of PMSM With Modified FCSMPC", *IEEE Transactions on Industrial Applications*, 52(6), pp. 4855–4864, 2016. <https://doi.org/10.1109/TIA.2016.2599902>
- [24] Geyer, T., Papafotiou, G., Morari, M. "Model Predictive Direct Torque Control - Part I: Concept, Algorithm, and Analysis", *IEEE Transactions on Industrial Electronics*, 56(6), pp. 1894–1905, 2009. <https://doi.org/10.1109/TIE.2008.2007030>
- [25] Lv, S. S., Lin, H. "Model Predictive Direct Torque Control for PMSM with Duty Cycle Optimization", In: Fifth International Conference on Instrumentation and Measurement, Computer, Communication and Control (IMCCC), Qinhuangdao, China, 2015, pp. 866–871. <https://doi.org/10.1109/IMCCC.2015.189>
- [26] Navardi, M. J., Milimonfared, J., Talebi, H. A. "Torque and Flux Ripples Minimization of Permanent Magnet Synchronous Motor by a Predictive-Based Hybrid Direct Torque Control", *IEEE Journal of Emerging and Selected Topics in Power Electronics*, 6(4), pp. 1662–1670, 2018. <https://doi.org/10.1109/JESTPE.2018.2834559>
- [27] Toso, F., De Soricellis, M., Bolognani, S. "Simple and robust model predictive control of PMSM with moving horizon estimator for disturbance compensation", *The Journal of Engineering*, 2019(17), pp. 4380–4385, 2019. <https://doi.org/10.1049/joe.2018.8052>
- [28] Preindl, M., Bolognani, S., Danielson, C. "Model Predictive Torque Control with PWM using fast gradient method", In: 2013 Twenty-Eighth Annual IEEE Applied Power Electronics Conference and Exposition (APEC), Long Beach, CA, USA, 2013, pp. 2590–2597. <https://doi.org/10.1109/APEC.2013.6520661>
- [29] Bolognani, S., Peretti, L., Zigliotto, M. "Online MTPA Control Strategy for DTC Synchronous-Reluctance-Motor Drives", *IEEE Transactions on Power Electronics*, 26(1), pp. 20–28, 2011. <https://doi.org/10.1109/TPEL.2010.2050493>
- [30] Shinohara, A., Inoue, Y., Morimoto, S., Sanada, M. "Correction of reference flux for MTPA control in direct torque controlled interior permanent magnet synchronous motor drives", In: 2014 International Power Electronics Conference (IPEC-Hiroshima 2014 - ECCE ASIA), Hiroshima, Japan, 2014, pp. 324–329. <https://doi.org/10.1109/IPEC.2014.6869601>
- [31] Kamel, H. M., Hasanien, H. M., Ibrahim, H. E. A. "Speed control of permanent magnet synchronous motor using fuzzy logic controller", In: 2009 IEEE International Electric Machines and Drives Conference, Miami, FL, USA, 2009, pp. 1587–1591. <https://doi.org/10.1109/IEMDC.2009.5075415>
- [32] Rebeiro, R. S., Uddin, M. N. "Performance Analysis of an FLC-Based Online Adaptation of Both Hysteresis and PI Controllers for IPMSM Drive", *IEEE Transactions on Industry Applications*, 48(1), pp. 12–19, 2012. <https://doi.org/10.1109/TIA.2011.2175876>
- [33] Xinghua, Z., Pengfei, C. "Efficiency optimization of direct torque controlled interior permanent magnet synchronous motor considering iron losses", In: 19th International Conference on Electrical Machines and Systems (ICEMS), Chiba, Japan, 2016. [online] Available at: <https://ieeexplore.ieee.org/document/7837241> [Accessed: 14 June 2020]

- [34] Biel, Z., Vittek, J., Hrkel, M. "Permanent magnet synchronous motor loss minimization control strategies", In: Proceedings of 9th International Conference, ELEKTRO, Rajecké Teplice, Slovakia, 2012, pp. 165–169.  
<https://doi.org/10.1109/ELEKTRO.2012.6225631>
- [35] Zhang, S., Zhou, X., Gao, D. "Strategy of efficiency optimization of PMSM-DTC system used for EVs", In: 2014 IEEE Conference and Expo Transportation Electrification Asia-Pacific (ITEC Asia-Pacific), Beijing, China, 2014, pp. 1–4.  
<https://doi.org/10.1109/ITEC-AP.2014.6940691>
- [36] Makwana, J. A., Agarwal, P., Srivastava, S. P. "Novel simulation approach to analyses the performance of in-wheel SRM for an Electrical Vehicle", In: 2011 International Conference on Energy, Automation and Signal, Bhubaneswar, India, 2011, pp. 1–5.  
<https://doi.org/10.1109/ICEAS.2011.6147103>
- [37] Lai, S. C., Ian Hill, C., Suchato, N. "Implementation of an Advanced Modelica Library for Evaluation of Inverter Loss Modeling", In: 2019 IEEE Texas Power and Energy Conference (TPEC), College Station, TX, USA, 2019, pp. 1–6.  
<https://doi.org/10.1109/TPEC.2019.8662144>
- [38] Saur, M., Piepenbreier, B., Xu, W., Lorenz, R. D. "Implementation and evaluation of inverter loss modeling as part of DB-DTFC for loss minimization each switching period", In: 16th European Conference on Power Electronics and Applications, Lappeenranta, Finland, 2014, pp. 1–10.  
<https://doi.org/10.1109/EPE.2014.6910691>
- [39] Guo, J. "Modeling and Design of Inverters using Novel Power Loss Calculation and DC-Link Current/Voltage Ripple Estimation Methods and Bus Bar Analysis", PhD, McMaster University, 2017. [online] Available at: <http://hdl.handle.net/11375/21231> [Accessed: 27 February 2021]
- [40] Morimoto, S., Tong, Y., Takeda, Y., Hirasa, T. "Loss minimization control of permanent magnet synchronous motor drives", IEEE Transactions on Industrial Electronics, 41(5), pp. 511–517, 1994.  
<https://doi.org/10.1109/41.315269>
- [41] Shinohara, A., Inoue, Y., Morimoto, S., Sanada, M. "Direct Calculation Method of Reference Flux Linkage for Maximum Torque per Ampere Control in DTC-Based IPMSM Drives", IEEE Transactions on Power Electronics, 32(3), pp. 2114–2122, 2017.  
<https://doi.org/10.1109/TPEL.2016.2569140>
- [42] Meher, H., Panda, A. K., Ramesh, T. "Performance enhancement of the vector control based Permanent Magnet Synchronous Motor drive using hybrid PI-Fuzzy logic controller", In: Students Conference on Engineering and Systems (SCES), Allahabad, India, 2013, pp. 1–6.  
<https://doi.org/10.1109/SCES.2013.6547542>
- [43] Zang, C. "Vector controlled PMSM drive based on fuzzy speed controller", In: 2nd International Conference on Industrial Mechatronics and Automation, Wuhan, China, 2010, pp. 199–202.  
<https://doi.org/10.1109/ICINDMA.2010.5538336>